Kerig.

UCRL- 94363
PREPRINT

HYDROLOGICAL PROPERTIES OF TOPOPAH SPRING TUFF - LABORATORY MEASUREMENTS

William Daily
Wunan Lin
Thomas Buscheck

Submitted to
Journal of Geophysical Research
Special Section on Nuclear Waste Management

December 1985

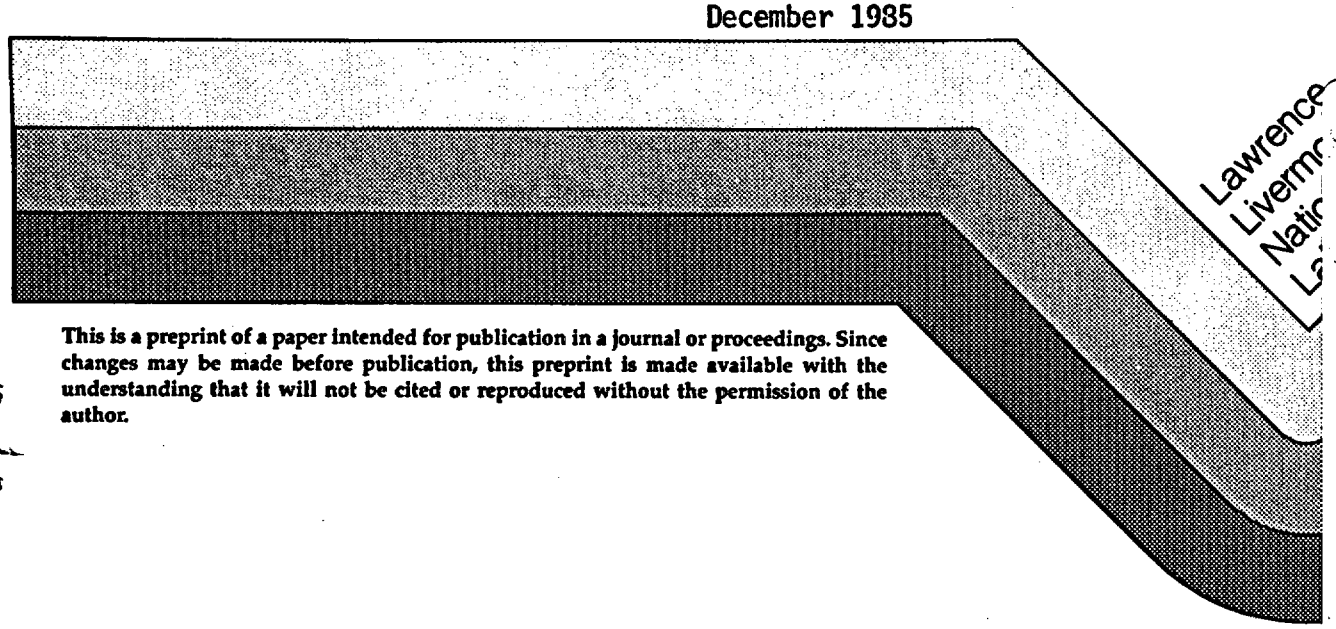

HYDROLOGICAL PROPERTIES OF TOPOPAH SPRING TUFF - LABORATORY MEASUREMENTS

William Daily

Wunan Lin

Thomas Buscheck

Lawrence Livermore National Laboratory

Livermore, CA 94550

December 1985

Submitted to Journal of Geophysical Research

Special Section on Nuclear Waste Management

HYDROLOGICAL PROPERTIES OF TOPOPAH SPRING TUFF - LABORATORY MEASUREMENTS*

ABSTRACT

The purpose of this work is to study the transport of water (both the liquid and vapor phases) in tuff from the Topopah Spring welded unit under conditions expected in the near field environment of a high level nuclear waste container. A naturally fractured sample of Topopah Spring tuff (approximately 8 cm in diameter and 10 cm long) from Yucca Mountain at NTS, Nevada, was studied using, as a pore fluid, natural ground water recovered from a well in which the principal producing horizon is the Topopah Spring Member. Confining pressure, sample temperature, and pore pressure were held at values that simulate expected in situ near field conditions shortly after emplacement of the container. Results of this work are comparable with results from previous similar experiments on 2.54 cm diameter samples of Topopah Spring tuff. During the more than six month experiment duration, water permeability decreased about three orders of magnitude. The most rapid measured permeability change (between about 600 and 100 μd) occurred when the sample temperature was increased from room temperature to 89°C. Subsequently, water permeability decreased in a fairly monotonic manner to a value of about 1 μd. This behavior probably resulted from a decrease in the aperture of the natural fracture, possibly reflecting transport and redeposition of silica (which was already present in the fracture). This process also resulted in a weak bonding of the sample halves. Previous experiments on two smaller

* Work performed under the auspices of the U.S. Department of Energy by the Lawrence Livermore National Laboratory under contract number W-7405-ENG-48.

naturally fractured Topopah tuff samples resulted in fracture healing presumably by the same mechanism. The degree of healing, indicated by bonded tensile strength and change in fluid permeability, seems to be sample dependent. The distribution of electrical resistivity indicates that the sample dehydrates and rehydrates nonuniformly. This is consistent with our findings on smaller samples. Computed impedance tomographs indicate that during each of the five subsequent dehydrations of the sample, water first left the matrix adjacent to the fracture surface, then escaped the sample through the fracture aperture. Drying then progressed into the matrix around the fracture. Rehydration of the dry sample was not quite the reverse of the dehydration process. Water initially entered the fracture along the fracture edge and the matrix was then wetted progressively from these points. However, the matrix was wetted also along paths apparently unrelated to fracture flow.

1. INTRODUCTION

Water, if present, may play a role in leaching and transporting radioactive materials in any underground nuclear waste repository. The Waste Package Task of the Nevada Nuclear Waste Storage Investigation (NNWSI) Project at Lawrence Livermore National Laboratory (LLNL) sponsors the study reported herein. One objective of NNWSI Project is to understand the near-field hydrological environment of a nuclear waste container [Glassley, 1986]. Our results describe the dehydration and rehydration processes in a core sample from the host rock of a potential nuclear waste repository at Yucca Mountain, Nye County, Nevada. The purpose of this study is to understand better the flow mechanisms through the welded tuff from the candidate horizon of the potential repository, with emphasis placed on water permeability and steam

permeability in single phase flow, dehydration and rehydration mechanisms, and water and steam flow through fractures and matrix.

In this study, measurements of electrical resistivity were used to monitor the movement of water in a sample of the candidate repository host rock (Topopah Spring welded unit) during several cycles of dehydration and rehydration. Water permeability and steam permeability were also measured when the naturally fractured sample was saturated with either water or steam. Experimental conditions were chosen to simulate the near-field environment of a radioactive waste container: 5.0 MPa hydrostatic confining pressure (to simulate the lithostatic pressure of about 230 m depth), pore fluid gauge pressures from zero to 2.5 MPa (unsaturated to saturated crustal conditions), temperatures between 20°C and 140°C (expected from ambient far-field to near the container emplacement wall). This study is a continuation of work that was reported by Lin and Daily [1984]; however, the present work is on a larger sample (8.75 cm instead of 2.54 cm diameter) and uses a recently developed technique, computed impedance tomography (CIT), to monitor water movement in the sample during the experiment.

2. EXPERIMENTAL PROCEDURES

2.1. SAMPLE DESCRIPTION AND PREPARATION

The rock studied was from the Topopah Spring Member of the Paint Brush Tuff. The sample was machined to a right circular cylinder (8.23 cm diameter and 10.09 cm length) from a core at the 343 m depth of borehole USW H-6 located in Yucca Mountain. The sample contained a natural healed fracture which approximately bisected the sample longitudinally. The fracture was reopened prior to the experiment. The sample axis was approximately

perpendicular to the bedding. The edges of the sample were beveled about 2 mm deep on both ends to facilitate a pressure tight match to metal end caps (see Fig. 1). Bulk density of the sample (dry and saturated) was calculated from measured dry and saturated weight and volume, and then apparent porosity was calculated. To obtain these data, the sample was dried in a vacuum oven at 30°C until its weight remained constant for at least one day (this required more than one week of drying). The sample was then placed in water from well J-13 (which penetrates a saturated zone of the Topopah Spring member about five miles horizontal distance from the repository site) at about 0.7 MPa until its weight remained constant for at least one day. Results of our measurements and other data of the sample are summarized in Table 1. Our measured apparent porosity of 8.45 percent is somewhat lower than the mean porosity for this unit of 14 percent reported by Montazer and Wilson [1984]. A welded tuff sample from the Topopah Member (hole USW G-1 at 376 m depth) was found, using mercury porosimitry, to have a mean pore diameter of about 0.02 microns and porosity of 6.54 percent [Knauss, 1986, private communication]. The petrology and geochemistry of densely welded tuff from the Topopah Spring Unit are reported in detail by Knauss [1984] and Bish, et al., [1981]. Bish and Vaniman [1985] report the mineralogical composition of a core sample from USW H-6 as shown in Table 2.

Platinum electrodes 0.08 mm thick, each about 6 mm square, were used for electrical resistance measurements. Four pairs of these electrodes were evenly spaced longitudinally on opposite sides of the cylindrical surface so that current was largely perpendicular to the sample axis. The electrode pairs were placed as close to the fracture plane as possible. Additionally, 14 electrodes (including 2 of those mentioned above) were evenly spaced

azimuthally in a ring around the sample at about two-fifths the sample length from the downstream end along the axis. This electrode arrangement, as well as the sample jacketing assembly, is illustrated in Fig. 1. Two ultrasonic piezoelectric transducers (compressional mode) with a natural frequency of 1 MHz were mounted in the Hastalloy end caps (Fig. 1); one served as the P-wave source, the other as the detector.

2.2. EXPERIMENTAL APPARATUS

The experimental apparatus consisted of three subsystems: the confining pressure system, the pore pressure system, and the electronics and computer system. Details of this apparatus were discussed by Daily and Lin [1985]. Hydrostatic confining pressure was maintained on the Teflon jacketed sample with a silicone-based oil. The sample was heated by external heating of the pressure vessel. The pore fluid pressure and the pore fluid pressure gradient across the sample were controlled manually by valves and monitored by pressure transducers. The pore fluid was introduced into the sample through one end cap and removed through the other. Flow rate was determined by measuring fluid volume exiting the sample in a given time interval when the flow rate became stable. The pore water came from well J-13 located to the east of Yucca Mountain where the Topopah Spring tuff lies below the water table. The Topopah Spring formation is the major producing horizon for this well. This water, with a resistivity of 33 ohm-meter at room conditions, was used in our experiments to simulate in situ rock water chemistry. The pore fluid pressure gradient was assumed to be linear over the sample length and was measured by one differential and two absolute pressure transducers (one at each end of the sample), and a Heise pressure gauge at the upstream end of the sample. The

electronics system was used to measure the electrical resistance, P-wave velocity, and to automatically maintain a constant confining pressure.

A commercial automatic conductance bridge was used to measure the resistance between the four electrode pairs arranged along the sample axis. Resistance of the 14 electrodes arranged azimuthally around the sample was monitored using a 4-electrode technique which will be described below. An Iron-Constantan thermocouple inside the pressure vessel adjacent to the sample, measured sample temperature. The piezoelectric transducer was driven by a 1-μs wide 90-V pulse. The output of the piezoelectric receiver was preamplified, and the pulse travel time was measured on a time delay oscilloscope.

2.3. COMPUTED IMPEDANCE TOMOGRAPHY

Rock resistivity is a strong function of water content. Therefore, a map of resistivity distribution within the core should indicate water distribution and changes in this map with respect to time should be indicative of water movement in the sample. Computed impedance tomography was the technique used to nonintrusively map the resistivity distribution, thereby monitoring water movement, within the sample during the course of the experiment.

The 14 electrodes arranged azimuthally and the four pairs arranged along the axis of the sample were used for the computed impedance tomography (CIT). To understand the technique, consider current flowing between two adjacent electrodes and the electrical potential measured, successively, between all other adjacent electrode pairs. The values of these potentials must reflect the distribution of current density within the core and thereby the distribution of electrical resistivity. In fact, these voltages can be

used to construct an image of resistivity distribution using a method similar to back projection used in computed x-ray tomography [Herman, 1979]. For the case schematically illustrated in Fig. 2, two adjacent electrodes are driven by a known current I, producing a potential distribution (assumed for a uniform resistivity distribution). The measured voltage difference between two other adjacent electrodes is used to assign a value of apparent resistivity to the region between the equipotentials terminating on these electrodes. Each of these apparent resistivity bands, one for each pair of drive current and sense voltage electrodes, are added together. The resulting image formed by such apparent resistivity back projections into the regions between equipotential lines, is the simplest image consistent with the data [Barber, et al., 1983]. The summed image is then spatially filtered to reduce the back projection smearing. The frequency of the drive current was 400 Hz and the voltage across the other adjacent pairs was measured using a commercial wave analyzer. This technique is being developed for use in medicine for various applications of in vivo imaging [e.g., Barber et al., 1983].

2.4. DATA ACQUISITION

The sample confining pressure was kept at approximately 5 MPa during the experiment duration - more than six months. Experimental history is summarized in Fig. 3. Initially, the rock was saturated and its water permeability was measured at 20°C, 96°C, and 145°C. For these measurements, the water was preheated and the pore pressure was kept above the equilibrium steam point at each temperature so that the pore fluid was liquid water. Then, the sample was subjected to 4-1/2 cycles of dehydration/hydration.

Experimental conditions were varied on each cycle and CIT was used to monitor water distributions at various stages of each cycle. Each dehydration was accomplished by opening both upstream and downstream pore water lines and allowing moisture to escape while sample temperature was held at about 140°C.

The first rehydration cycle was accomplished by lowering the temperature to about 89°C and introducing water to one end of the rock (labeled upstream on Fig. 1) at a pressure of about 0.1 MPa (gauge pressure). Downstream pore pressure was zero. Rehydration for the second cycle was at a sample temperature of 138°C and upstream pore pressure of approximately 2.5 MPa. Rehydration for cycle three was at 130°C sample temperature and about 0.2 MPa upstream pore pressure. Because the steam point for water at 0.2 MPa is about 104°C, steam was the predominant saturant during this cycle. Rehydration for the last cycle was accomplished at a sample temperature of 90°C and approximately 0.1 MPa upstream pore pressure, similar to cycle one, except that the water was introduced into the previously downstream end of the sample (the water flow direction was reversed). The fifth cycle consisted only of dehydration at 135°C until no systematic changes in resistivity of the rock were measured - a condition which was assumed to imply loss of all water from the connected pores in the sample. The above experimental sequence was chosen to yield an adequate database on the hydraulic characteristics of this sample and to facilitate comparison of this data to similar data available on smaller core samples of Topopah Spring tuff [Lin and Daily, 1984].

3. PERMEABILITY

The measured permeability values are summarized in Table 3. Each of these values is an average of several measurements taken at a specific experimental condition. Individual measurements during the history of the experiment are shown in Fig. 4. Each permeability value was determined by maintaining a temporally constant pore fluid pressure gradient across the sample and measuring at the downstream end the volume of water that moved through the sample in a known time. Assuming the pore pressure gradient is linear, the permeability k in darcys is

$$k = \frac{(\Delta V/\Delta t)\mu}{A(\Delta P/\Delta L)}$$

where

$\Delta V/\Delta t$ is the flow rate in cm^3/s,

μ is the fluid viscosity in cp,

A is the sample cross sectional area in cm^2, and

$\Delta P/\Delta L$ is the pore pressure gradient in atmosphere/cm.

Whether designated as "steam" or "water," each permeability value was calculated from the observed equivalent flow rate of liquid water from the sample. Note that water permeability was measured with pore pressure above the steam point at the sample temperature, therefore, we assume a liquid phase in the pore volume. For steam flow, the pore pressure was below the steam point at the sample temperature so that vapor phase is the pore fluid. For steam permeability, the fluid volume was obtained by converting the water volume collected, to a steam volume at the sample temperature and pore

pressure. The actual pressure gradient for this case is unknown, so we have assumed a linear gradient and used the above equation to calculate an effective steam permeability.

Calculation of permeability requires measurements of three quantities, each of which has a measured accuracy that will result in an overall accuracy in the calculated value. Measurement of pore fluid volume exiting the sample had an uncertainty of about 10 percent, and the measurement of time had an uncertainty of less than 1 percent. Although considerable effort was exerted to maintain constant pore pressure during the measurement, we can only estimate the pressure gradient accuracy to be from 2 to 5 percent. Therefore, the calculated permeability values greater than about 10 μd should have an uncertainty of 12 to 15 percent. The higher permeabilities are the more accurate. Larger uncertainties in fluid volume and pore pressure measurements result in increased uncertainties for permeabilities less than 10 μd, where uncertainties may approach 50 percent. The temperature dependence of water or steam viscosity was accounted for in the permeability calculations [Eisenberg and Kauzmann, 1969].

The initial room temperature permeability of this fractured tuff sample, 1400 μd, is more than three orders of magnitude greater than that of intact samples under the same experimental conditions [Lin and Daily, 1984]. The initial permeability decreased to 700 μd after a pore pressure cycle from 2.5 MPa to atmospheric pressure while the confining pressure was at 5.0 MPa. Large permeability through a fracture has been reported in other rocks [Lin, 1978; Daily and Lin, 1985]. However, permeability of this tuff sample decreased about an order of magnitude with the first increase in sample temperature to 89°C. This is consistent with our previous observation on

smaller samples also containing reopened natural fractures [Lin and Daily, 1984]. Sample permeability was not strongly correlated with further temperature changes. Therefore, it is unlikely that the initial decrease in permeability was due to aperture closure from mechanical deformation at the elevated temperature. Instead, we attribute it to fracture healing. Following this initial permeability decrease, there was a rather steady decline in permeability from about 100 μd to about 1 μd over the six month experiment duration. Similar characteristic permeability changes were seen in previous experiments on the smaller Topopah tuff samples. This phenomenon was likely due to silica redeposition in the fracture which changed the effective aperture. This will be discussed in more detail later.

Steam permeability (at sample temperature of 140°C) was between 20 and 30 μd. This range of values is similar to the water permeabilities measured before and afterward. There is no evidence that the steam and water permeabilities are substantially different in fractured Topopah Spring tuff. Although the reported steam permeability of a smaller sample [Lin and Daily, 1984] was only 3.9 μd, this probably reflects sample variation and the fact (as other data suggest) that the fracture in the smaller sample had healed more completely by the time this measurement was made.

4. DEHYDRATION AND REHYDRATION PROCESSES

As already mentioned, one of our experimental measurements is the distribution of electrical resistivity in the sample as a function of time. Figure 5 shows the resistivity of the sample measured between electrode pair 1-2, the upstream electrode pair (as shown in Fig. 1, the electrodes closest to the end where water is introduced). The major variations of resistivity

shown in this figure correspond to drying, wetting, and temperature changes during various stages of the experiment. Initially, the sample was saturated with J-13 water and the resistivity was about 700 ohm-m (hour 290). The first drying period was between hour 290 and hour 540. The rapid decrease of resistivity at hour 540 corresponds to the introduction of J-13 water at 0.2 MPa pressure. The second drying period was between hours 650 and 730. The rapid decrease in resistivity following the second drying period was due to the addition of water at 140°C and 2.5 MPa pressure to the sample. The third drying period was at 138°C and started at hour 1060. Then, at about hour 1360, steam at 0.2 MPa pressure (preheated water at a temperature above the steam point) was added to the sample. The fourth dehydration at 1550 hours was also accompanied by a large resistivity increase. During this drying, sample temperature was lowered to 91°C. Then, at 1780 hours, water was introduced at 0.1 MPa pressure to the opposite end of the rock (which, until this point, had been the downstream end). The lower recovery rate of resistivity to values indicative of saturated rock is probably due to three effects: 1) Electrode pair 1,2 is at the downstream end of the rock for this rehydration and may be expected to react more slowly, especially if the wetting front is highly nonuniform, 2) the first water rehydration (hour 540) was at an upstream pressure of about 0.2 MPa (roughly twice that for this cycle) and similarly, the rehydration at 920 hours was at 2.5 MPa water pressure, and 3) sample permeability had decreased substantially by this point in the experiment.

The sample was kept saturated at 91°C from hours 2160 to 4280 (88 days) to monitor permeability changes which might indicate fracture healing or related phenomena. Notice (Fig. 4) that the water permeability eventually

reached about 1 μd [the value reported for intact welded tuff by Montazer and Wilson, 1984] - about three orders of magnitude lower than the original value, but about one order of magnitude larger than that of a smaller intact (unfractured) Topopah Spring tuff sample (2.54 cm dia.) measured previously [Lin and Daily, 1984]. The last dehydration was started at hour 4280 with a sample temperature of 134°C and continued for 240 hours. When sample resistivity became stable, drying was assumed complete. The sample was then removed from the experimental apparatus and weighed to ascertain that the residual saturation was 8.7 percent. (Assuming that the pore fluid neither deposited nor leached material from the rock.) This probably was the percent residual saturation at the conclusion of each drying stage of the experiment.

As noted in Fig. 3, CIT data was collected during critical stages of the experiment, especially during hydration and dehydration, to establish spatial and temporal distribution of water in the sample during these transient conditions. A total of 39 individual images were made. These are shown in Fig. 6.

Each image is a map reflecting the resistivity distribution in the plane near the electrode ring. These images can represent water distribution because the rock resistivity is inversely related to water content (Fig. 5). The first three images show a resistivity distribution in the saturated sample at three different temperatures which are relatively uniform in comparison to those of intermediate saturation levels. Image 4, made after 21 hours of drying at 134°C, shows a band of high resistivity coincident with the fracture trace in the electrode plane. In subsequent dehydration periods when images were taken more frequently, this band is even better delineated (images 13, 14, 21, 22, 43, and 44). Note that this pattern occurs only during the

initial stages of each dehydration cycle - later in the process the images show a pattern apparently unrelated to the fracture location. There are three images of this latter stage in dehydration (14, 21, and 22) and the patterns show some similarity. From these data, we conclude that initial water loss from the sample is through the fracture. Water leaves the matrix by preferentially moving towards the fracture where it then moves axially along the fracture and finally exits the sample. Water will preferentially boil off from areas with the largest pore size which are in proximity to the pressure sink (i.e., the fracture). Generally, the high permeability areas are in more direct hydraulic communication with the pressure sink in the fracture and the areas with smaller pore space will tend to hold liquid water by capillary suction. This vapor flow tends to move through the high permeability zones, bypassing the low permeability areas which are at a higher saturation. The dry region around the fracture expands with time, but at some point (e.g., by the 42nd hour of drying in the second dehydration cycle), the water distribution is not controlled by the fracture. It is possible that the sample size influences drying at this stage because the characteristic distance from the drying front to the fracture is nearly equal to the characteristic distance from the drying front to the sample exit. By hour 42 of the second dehydration, the drying fronts from the sample exit and fracture coalesce so that the CIT image exhibits a decreasing influence of the fracture and an increasing influence of the ends. In other words, dehydration is primarily from the flat end faces of the cylindrical sample. These images also corroborate the fracture permeability change during the experiment. This can be concluded from the fact that the sample is much dryer after 21 hours in the first dehydration (image 4) than after 24 hours in the third dehydration

(image 22). When dry, CIT shows the core to be fairly uniform in resistivity (e.g., image 5). The highly resistive core in this image and in other images of the dry sample are probably an artifact of the poor signal-to-noise ratio which happens when the sample resistivity is so high. It should be noted that dehydration of the sample was not always by gradual water loss. Occasional bursts of steam escaped the sample with sufficient impulsive force to startle someone standing near the pressure vessel. Although the effects of these events on sample properties are not known, there was no evidence of additional macroscopic or microscopic fracturing of the sample when it was examined after the experiment.

During rehydration, liquid water does not appear to enter the sample in exactly the reverse process by which it left as vapor during dehydration. This irreversibility probably is a consequence of hysteresis in the liquid-vapor characteristic curves [Freeze and Cherry, 1979]. Image 6 shows that water (at approximately 0.1 MPa upstream pressure) initially moves into the image plane through the fracture along one edge of the sample. A few hours later (image 8) water appears at the opposite end of the fracture along the other side of the sample. The apparent enhanced hydraulic conductivity along the fracture edges may be from mechanical damage to the fracture edge when it was pried apart. The teflon sleeve in contact with the sample surface may not completely seal at this point allowing the water to leak past into the CIT image plane. From image 8 we conclude that water enters the matrix around these locations before it has reached the image plane along the full cross section of the fracture. Water is also apparently entering the matrix along the lower left part of the sample as shown in images 8 and 9. A similar pattern is seen in images 16 (another water saturation but at 2.4 MPa water

pressure), 36, 37, and 38 (water saturation at 0.1 MPa but introduced into the other end of the sample). Apparently, during wetting, liquid water preferentially moves into regions of high permeability - a phenomenon known as viscous fingering. This flow will become more spatially uniform as water is imbibed into adjacent lower permeability regions of higher capillary suction.

Images 28 through 34 were made during steam saturation (about 0.2 MPa water pressure and 138°C) and subsequent dehydration. Interpretation of these images in terms of steam distribution is uncertain because the relationship between rock resistivity and steam content has not been clearly established. If we assume a similar relationship as that between resistivity and water content, some interesting observations follow. Neither the steam saturation nor drying process (both vapor dominated flow) is similar to the saturation by liquid water (liquid dominated flow). The sample matrix does not become as uniformly saturated by steam as when saturated by water. This is a likely consequence of the weak capillary forces inherent to steam and the variations of capillary effects with the steam quality. These smaller capillary forces are not sufficient to overcome the local variation in permeability, with the result that steam bypasses (viscous fingering) the low permeability regions.

The CIT discussed above gives information only near a plane defined by the ring of electrodes. The four pairs of electrodes arranged linearly parallel to the sample axis can yield information about water distribution along the sample axis in the plane of the fracture. Some of the data from these electrodes has been analyzed similarly to that by Lin and Daily [1984] on 2.54 cm diameter samples of Topopah Spring welded tuff, so that a comparison can be made between the samples. Figure 7 shows the results of that analysis where the plane containing the eight electrodes is divided into

ten areas, each containing the predominant current of an electrode pair. Each area is shaded to indicate the relative resistivity change between nearly saturated and nearly dry conditions. Water at 0.1 MPa pressure is introduced to the upstream end of the sample at hour 540. During the first three hours, water movement is primarily along one side of the sample. (Remember that these electrodes are aligned so that current flow is primarily parallel to the fracture aperture.) This is consistent with our previous conclusions from the CIT images which showed water "fingering" first into the fracture along one side of the sample. However, after this time (roughly speaking after the water front passes the CIT electrode ring) the water front is distributed fairly evenly across the sample, perhaps from smearing of the fingered front due to capillarity. This uneven movement (or viscous fingering) of the water front was observed to be more pronounced on a 2.54 cm diameter fractured tuff sample [Lin and Daily, 1984].

5. FRACTURE HEALING

As discussed earlier, the water permeability decreased by almost three orders of magnitude during the course of the experiment. When the sample was removed from the pressure vessel, the fracture was found to be healed so that the sample pieces were loosely bonded together. This same phenomenon had been reported in two naturally fractured 2.54 cm diameter samples [Lin and Daily, 1984]. One of these smaller samples had healed to such an extent that it had about half the tensile strength (5 MPa, measured by Brazilian testing) of an intact sample (9 MPa). In contrast, the larger sample studied here separated along the fracture when pulled apart by hand.

As mentioned earlier, the sample initially contained a reopened naturally healed fracture which was coated with white silica. The healing probably occurred when this secondary mineral was relocated on the fracture surface by flow of water above about 90°C. The water solubility of silica is a function of pressure, temperature, water pH, and the concentration of several other species (which also depend on pressure and temperature) [Helgeson, 1974; Walther and Helgeson, 1977]. It may be that as the temperature reaches 90°C, the water becomes saturated with respect to silica because of concentration changes in other species, pH changes, etc. As water moves slowly through the fracture, precipitation of silica causes closure of the aperture. Scanning electron microscopy could be interpreted to indicate deposition of silica (see Fig. 8) similar to (but to a lesser extent than) that found on the smaller samples of Lin and Daily [1984]. Verma et al. [1985] reported silica migration from within the matrix itself due to water solubility variations related to thermal gradients in the sample. This process seems unlikely in the present case because thermal gradients were small (less than 1-2°C across the sample length) and previous experiments [Lin and Daily, 1984] on an intact Topopah Spring tuff sample showed no measurable indications of silica solubility from the matrix at high temperatures. This healing is more likely caused by a redistribution of silica already in the fracture. One possibility is the transport of silica by hot water flow and deposition at nucleation points. Deposition could have been initiated by small gradients in species concentration, ph, or temperature. It is also possible that reopening of the fracture prior to the experiment precipitated its later healing. In opening the fracture, it is likely that some of the silica filling the aperature was loosened. Additional material was loosened and some pulverized in mating of

the two sample pieces together again. This results in several possible effects. First, the fracture aperture is larger than it was originally. In particular, granular "shims" of silica may support the sample pieces at different contact points. Second, the silica distribution may be less uniform. Third, any pulverized silica has an enhanced specific surface area, and thereby a possible enhanced rate and extent of solubility. Additionally, pulverized silica may be relocated (by water flow) in such a way as to reduce permeability. Any chemical erosion of these silica "shims" would reduce the mechanical support of the opposing fracture faces and result in fracture closure. If fracture permeability is related to the cube of the effective aperture [Gangi, 1978], only a small reduction in aperture width is necessary for a large reduction in measured permeability.

As previously discussed, some of the CIT images show evidence for enhanced fracture permeability at the fracture edge. If this is due to a small amount of mechanical damage to the fracture when it was opened prior to the experiment, the effective aperture would be larger and any original silica coating may be lost along the fracture edge. Both of these would result in reduced fracture healing along the fracture edge from any silica redistribution mechanism that may have been operative during the experiment.

6. SUMMARY AND CONCLUSIONS

Water transport properties of fractured Topopah Spring tuff were studied over a six month period with the sample at conditions designed to simulate the near field pressure and thermal environment of a high level nuclear waste container. We summarize here the principal conclusions from this work.

Electrical measurements of the sample were found very useful to delineate water content and distribution in the sample during the experiment. In particular, CIT was used to map, in sample cross section, water movement near a natural fracture. When dehydrating at 135°C from a saturated state, the rock loses water preferentially along the fracture. Apparently, water in the matrix along the fracture escaped first. The matrix dried progressively away from and uniformly along the length of the fracture surface. During the later stages of dehydration within each drying cycle, the impedance images seem to be influenced by dehydration from both the sample ends and the fracture.

Rehydration of the dry sample was not the reverse of the dehydration process. Water front movement was fairly nonuniform, occurring first through the fracture along the sides of the sample perhaps due to damage to the fracture edges when the sample was pried apart. The matrix was wet from these source points in the fracture, but also by movement through an unfractured part of the matrix (presumably by capillarity). These conclusions are compatible with the results of Lin and Daily [1984] from studies of smaller samples of Topopah Spring tuff.

Sample permeability decreased by more than three orders of magnitude (1400 to 1 ud) during the six month experiment. The largest decrease occurred when the sample temperature was first raised above 90°C. Apparently, the decrease of permeability was caused by fracture healing. We have observed the similar phenomena on three naturally fractured Topopah Spring tuff samples -- two 2.5 cm diameter samples [Lin and Daily, 1984] and the 8.75 cm diameter sample discussed herein. The extent of healing, attendant fracture bonding strength and permeability change appears to be sample dependent.

ACKNOWLEDGMENTS

The authors are grateful to J. Carbino, M. Christensen, and J. Beatty for technical support, and to J. Lytle for implementation of impedance imaging. Helpful discussions with V. Oversby, W. Glassley, A. Duba, K. Knauss, and H. Heard are gratefully acknowledged. This work was supported by the Waste Package task of the Nevada Nuclear Waste Storage Investigation Project at Lawrence Livermore National Laboratory.

REFERENCES

Barber, C. C., B. H. Brown, and I. L. Freeston, "Imaging Spatial Distributions of Resistivity Using Applied Potential Tomography," Electron. Lett., 19, 933-935, 1983.

Bish, D. L. and D. T. Vaniman, Mineralogic Summary of Yucca Mountain, Nevada, Los Alamos National Laboratory Report LA-10543-MS, 1985.

Bish, D. L., F. A. Caporuscio, J. F. Copp, B. M. Crowe, J. D. Purson, J. R. Smyth, and R. G. Warren, Preliminary Stratigraphic and Petrologic Characterization of Core Samples From USW-G1, Yucca Mountain, Nevada, Los Alamos National Laboratory, Los Alamos, NM, LA-8840-MS, 1981.

Daily, W. D. and W. Lin, "Laboratory Determined Transport Properties of Berea Sandstone," Geophysics, 50, 775-784, 1985.

Eisenberg, D. and W. Kauzmann, The Structure and Properties of Water, Oxford Press, New York, NY, 1969.

Freeze, R. A. and J. A. Cherry, Groundwater, Prentice Hall, New Jersey, 1979.

Gangi, A. F., "Variation of Whole and Fractured Porous Rock Permeability with Confining Pressure," Int'l. J. of Rock Mech. Mining Sci. and Geochem. Absts., 249-257, 1978.

Glassley, W., Reference Waste Package Environment Report, Lawrence Livermore National Laboratory, UCRL-53726, in press, 1986.

Helgeson, H. C., "Chemical Interaction of Feldspars and Aqueous Solutions," in The Feldspars, W. S. MacKinzie and J. Zussman eds., Manchester Univ. Press, pp. 184-217, 1974.

Herman, G. T. (Ed.), "Image Reconstruction from Projections: Implementation and Applications," Topics in Applied Physics, 32, Springer-Verlag, Berlin, 1979.

Knauss, K. G., Petrologic and Geochemical Characterization of the Topopah Spring Member of the Paintbrush Tuff: Outcrop Samples Used in Waste Package Experiments, Lawrence Livermore National Laboratory, Livermore, CA, UCRL-53558, 1984.

Lin, W., Measuring the Permeability of Eleana Argillite From Area 17, Nevada Test Site, Using the Transient Method, Lawrence Livermore National Laboratory, Livermore, CA, UCRL-52604, 1978.

Lin, W. and W. Daily, Transport Properties of Topopah Spring Tuff, Lawrence Livermore National Laboratory, UCRL-53602, 1984.

Montazer, P. and W. E. Wilson, Conceptual Hydrologic Model of Flow in the Unsaturated Zone, Yucca Mountain, Nevada, U.S. Geol. Survey, Water-Resources Report 84-4345, 1984.

Verma, A. K., K. Pruess, C. F. Tsang, and P. A. Witherspoon, "A Study of Two-Phase Concurrent Flow of Steam and Water in an Unconsolidated Porous Medium," Heat Transfer in Porous Media and Particulate Flows, the 23rd National Heat Transfer Conference, Denver, CO, August, 135-143, 1985.

Walther, J. V. and H. C. Helgeson, "Calculations of the Thermodynamic Properties of Aqueous Silica and the Solubility of Quartz and Its Polymorphs at High Pressure and Temperature," Amer. J. Sci., 277, 1315-1351, 1977.

FIGURE CAPTIONS

Figure 1. Schematic of sample assembly. The four electrodes arranged axially were matched by electrodes diametrically opposite on the cylinder. The 14 electrodes (including 2 in the axial set), evenly spaced azimuthally around the sample, were used for computed impedance tomography (CIT). The fracture approximately bisected the 8.23 cm diameter and 10.0 cm long sample. A thermocouple was located outside the jacket but next to the sample. The assembly was immersed in a silicon-based oil which provided the hydrostatic confining pressure. Heating was by an electrical resistance heater external to the pressure vessel.

Figure 2. Schematic of data acquisition for CIT. For each of the 14 source configurations (adjacent pairs), voltage was measured on the remaining 11 adjacent electrode pairs. Potential surfaces associated with each sensor electrode are shown in cross section.

Figure 3. Experiment history. Sample temperature and water content is given as a function of time during the more than six month experiment duration. CIT data were taken, at times indicated, usually during changes in sample water content.

Figure 4. Fluid permeability plotted as a function of time.

Figure 5. Electrical resistivity measured at electrodes 1 and 2 as a function of time. During the following intervals, a resistor of 10 MΩ was connected parallel to the electrodes: 301-511, 631-901, 1041-4281, 4331-4541. This procedure was necessary to monitor changes in sample resistance at values above the range of our resistance bridge. The resistivity scale is incorrect for data during these time intervals.

Figure 6. Computed impedance tomographs of the Topopah Springs tuff sample. Each color coded value in the image is proportional to the apparent resistivity of that point in the sample near the plane of the 14 electrodes. Each horizontal row depicts a separate dehydration or hydration sequence. In the upper left corner of each image the status within the sequence is denoted: sat = fully saturated, dryg = drying, dry = fully dry, wtg = wetting, stm wtg = wetting with steam, stm sat = saturated with steam, dryg stm = drying from steam saturation, wt dsm = wetting by introduction of water into the nominally downstream end of the sample. Also in this corner is a sequential number identifying each image. The lower left number associated with each image is the Celcius temperature of the sample. For those data taken when the sample was dehydrating or hydrating, the number in the upper right corner gives the hours from the beginning of the process. For the wetting sequences, the number in the lower right corner is the upstream pore fluid pressure in MPa. Some images are shown twice since they represent both the end of one sequence and the beginning of the next. Approximate location of the fracture in the image plane is shown on image 21.

Figure 7. Spatial distribution of electrical resistivity near the plane containing the eight electrodes arranged in four pairs parallel to the sample axis. This plane is close to the fracture (see Fig. 1). The plane is divided into 10 areas, each containing the predominant current of an electrode pair. Each area is shaded to indicate resistivity difference for that area (from when the sample was nearly saturated and when it was nearly dry) and therefore should reflect the distribution of water as it flows through the rock. Below each part is the time in hours from the introduction of water at about 0.1 MPa pressure to the upstream (left side here) end. Sample temperature was 87°C to 89°C.

Figure 8. Scanning electron micrograph of the fracture surface at the conclusion of the experiment. The layered material is silica, apparently moved by water transport from other locations on the surface and redeposited in a manner to affect fluid permeability.

TABLE 1.

Dimensions (diameter x length in cm), dry bulk density (g/cc), effective porosity (%), and ultrasonic velocity (km/s) for Topopah Spring tuff sample.

Dimensions	8.23 x 10.10
Dry bulk density	2.32
Effective (connected) porosity	8.45
Ultrasonic velocity (compressional wave)	3.2

TABLE 2.

Mineralogic summary (percent by weight) of core from USW H-6 after Bish and Vaniman [1985].

Sample	Depth (m)	Smectite	Mica	Clinoptilolite	Analcime	Quartz	Cristobalite	Alkali Feldspar	Glass	Other
1092.4	333.0	trace	trace	-	-	20 ± 5	9 ± 5	70 ± 10	-	-
1128.8	344.1	trace	~1	-	-	21 ± 5	12 ± 5	66 ± 10	-	-
1149.2	350.3	trace	trace	-	-	16 ± 5	15 ± 5	69 ± 10	-	-

TABLE 3.

Summary of fluid permeability for Topopah Spring tuff sample.

Pore Fluid	Temperature, °C	Approximate Time Period, Hours	Average Permeability, μd
Water	20	80 - 200	907
	89	200 - 220	105
	99	220 - 260	77
	140	260 - 280	56
	89	490 - 590	45
	134	590 - 650	47
	138	890 - 1040	41
Steam	138	1330 - 1530	26
Water	91	2070 - 4170	(30-0.2)

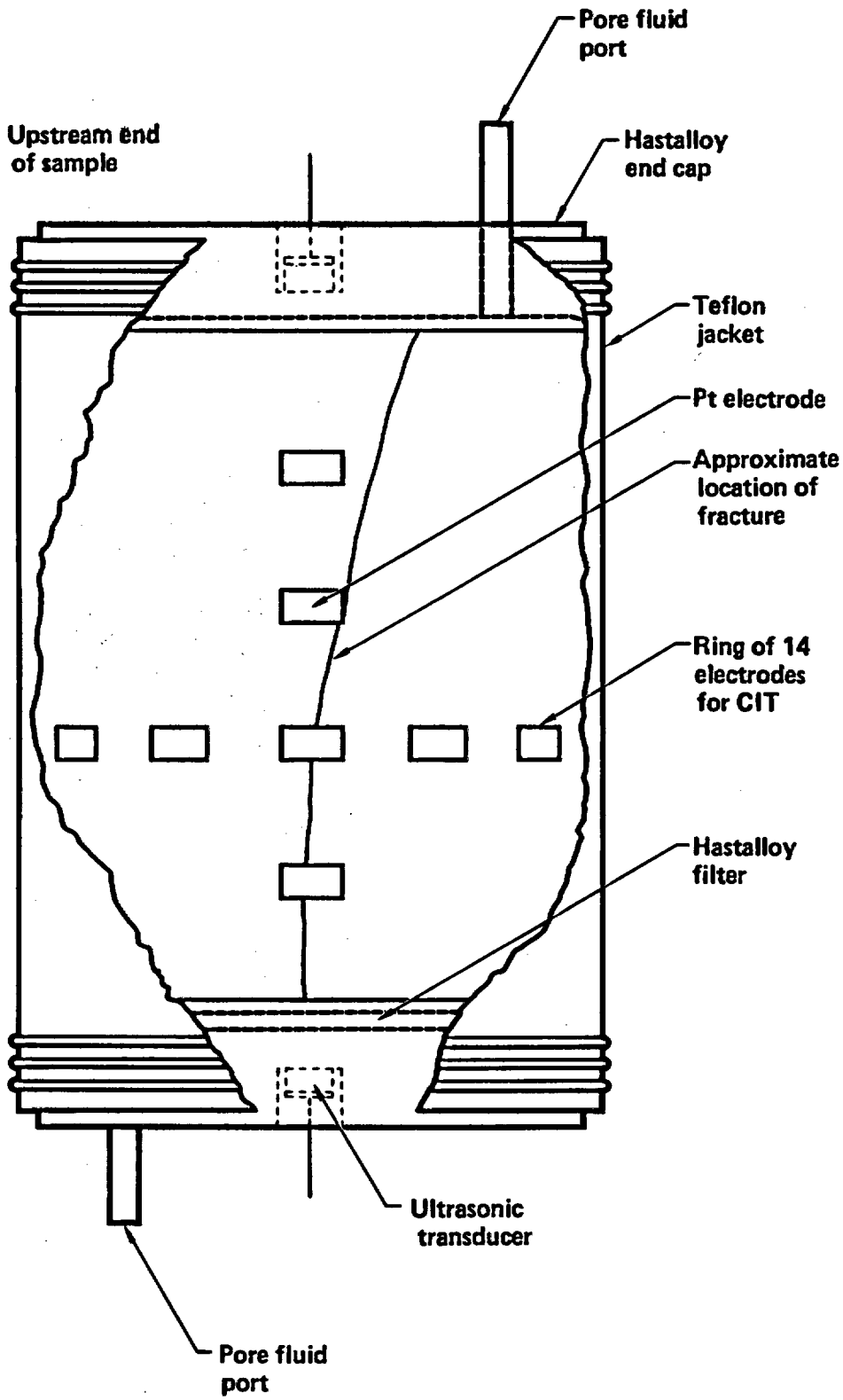
Pore fluid port
Upstream end of sample
Hastalloy end cap
Teflon jacket
Pt electrode
Approximate location of fracture
Ring of 14 electrodes for CIT
Hastalloy filter
Ultrasonic transducer
Pore fluid port

Fig 1

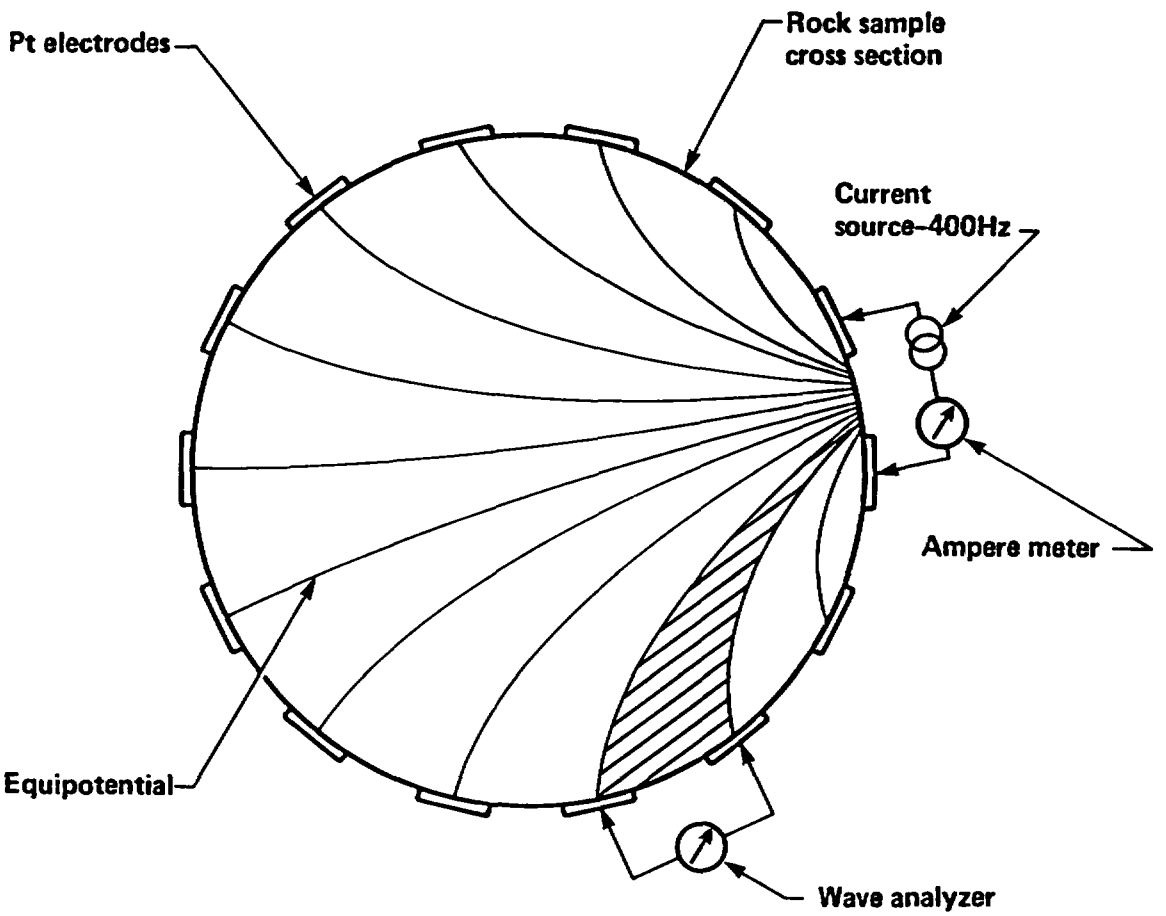
Pt electrodes
Rock sample
cross section
Current
source-400Hz
Ampere meter
Equipotential
Wave analyzer

Fig 2

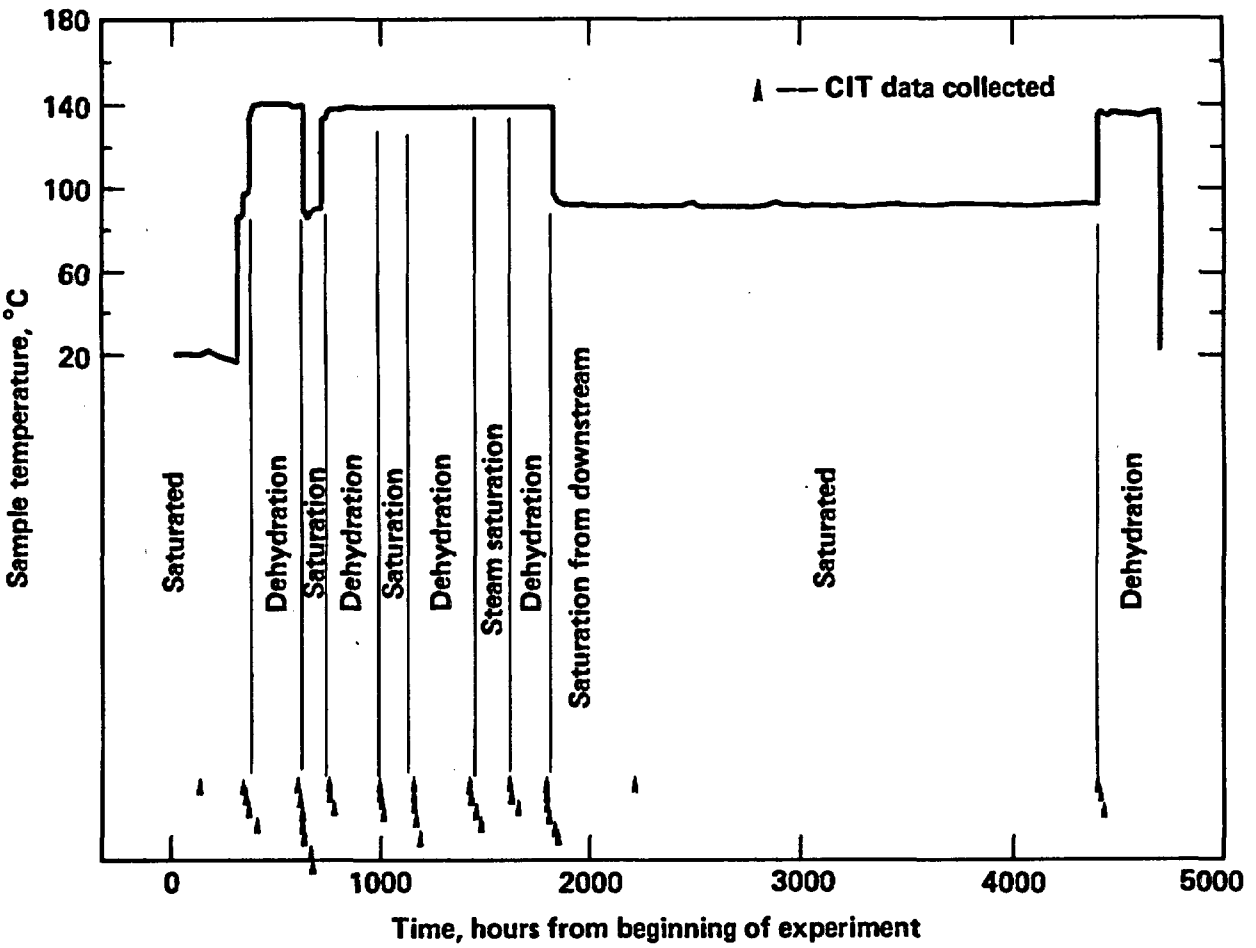
180
140
100
60
20
Sample temperature, °C
▲ — CIT data collected
Saturated
Dehydration
Saturation
Dehydration
Saturation
Dehydration
Steam saturation
Dehydration
Saturation from downstream
Saturated
Dehydration
0
1000
2000
3000
4000
5000
Time, hours from beginning of experiment

Fig 3

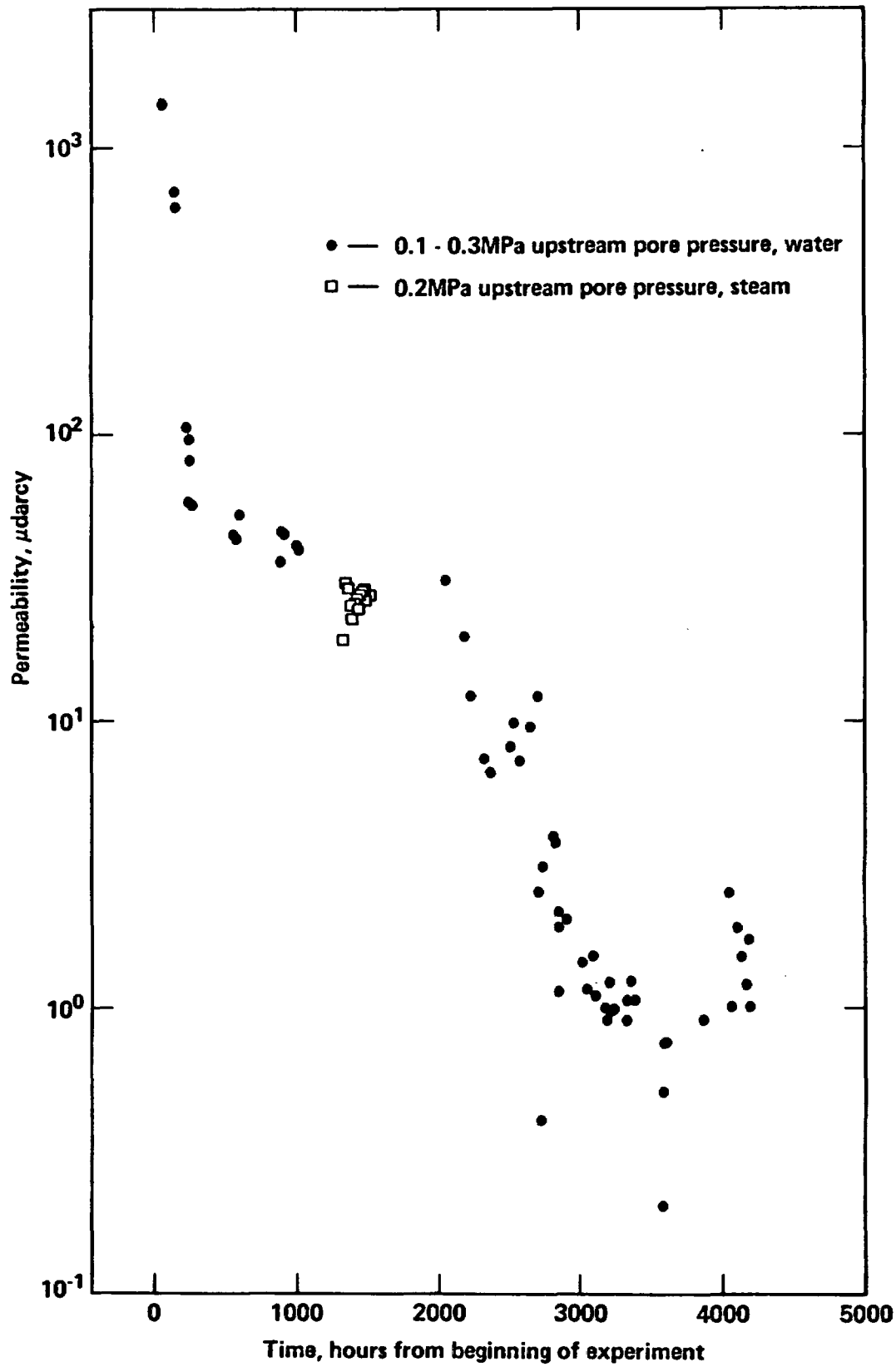
● — 0.1 - 0.3MPa upstream pore pressure, water
□ — 0.2MPa upstream pore pressure, steam
Permeability, μdarcy
10³
10²
10¹
10⁰
10⁻¹
0
1000
2000
3000
4000
5000
Time, hours from beginning of experiment

Fig 4

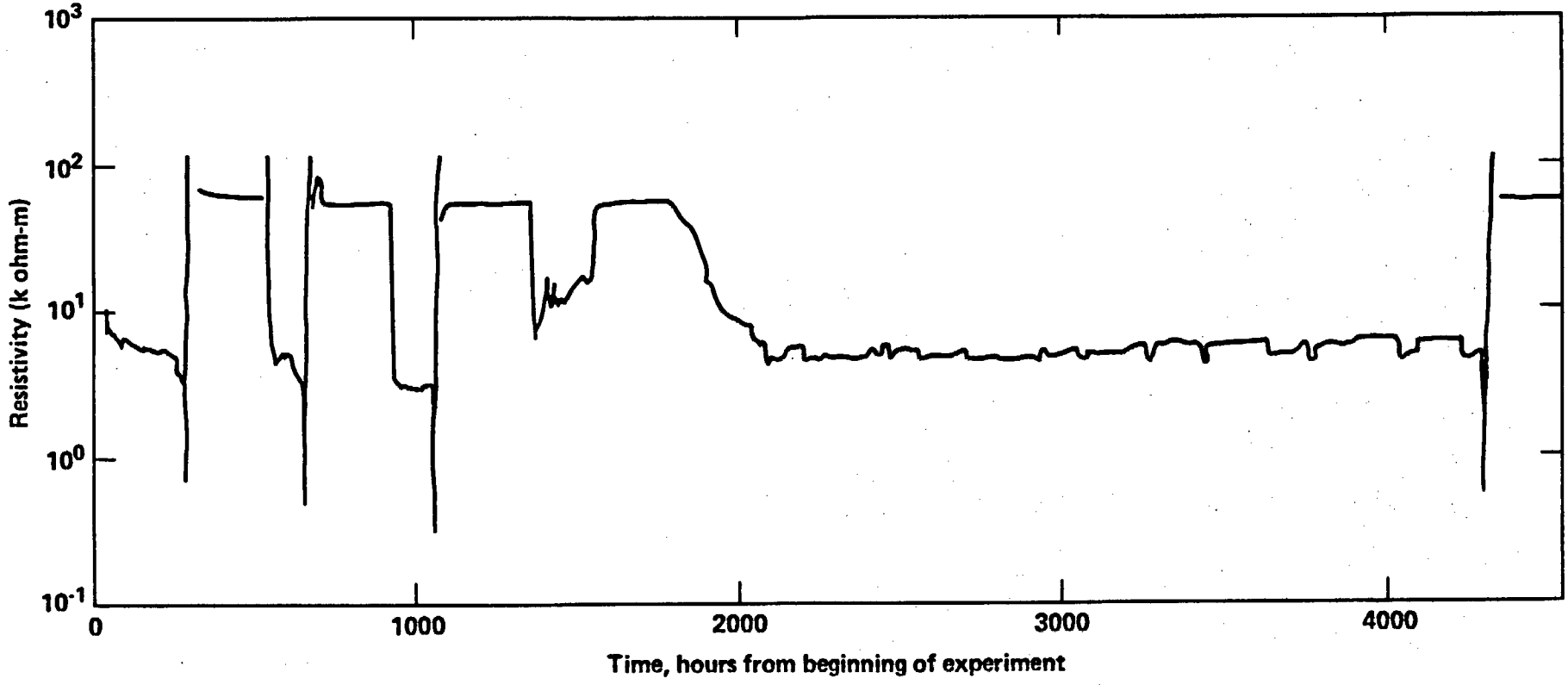
10^3
10^2
10^1
10^0
10^{-1}
Resistivity (k ohm-m)
0
1000
2000
3000
4000
Time, hours from beginning of experiment

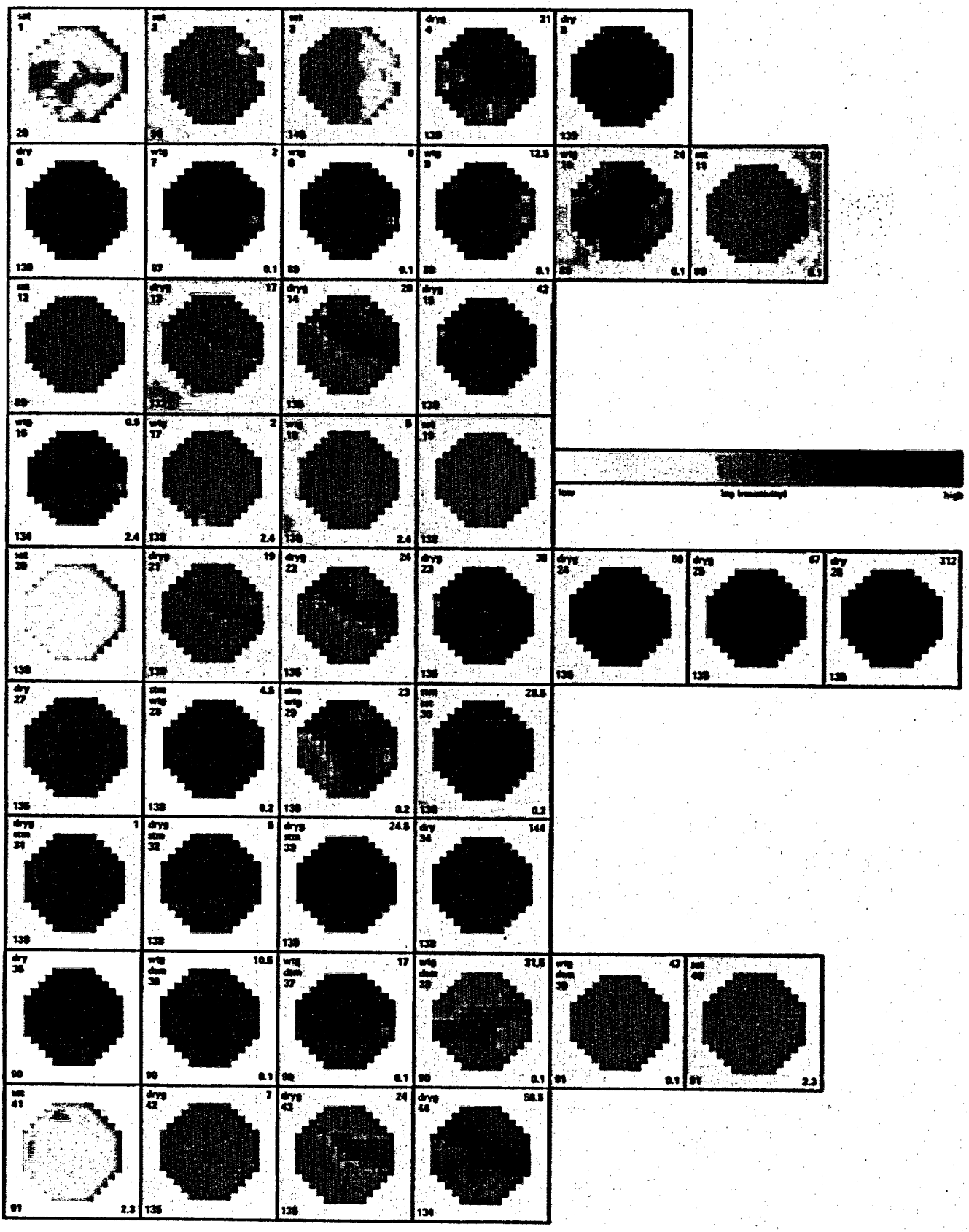

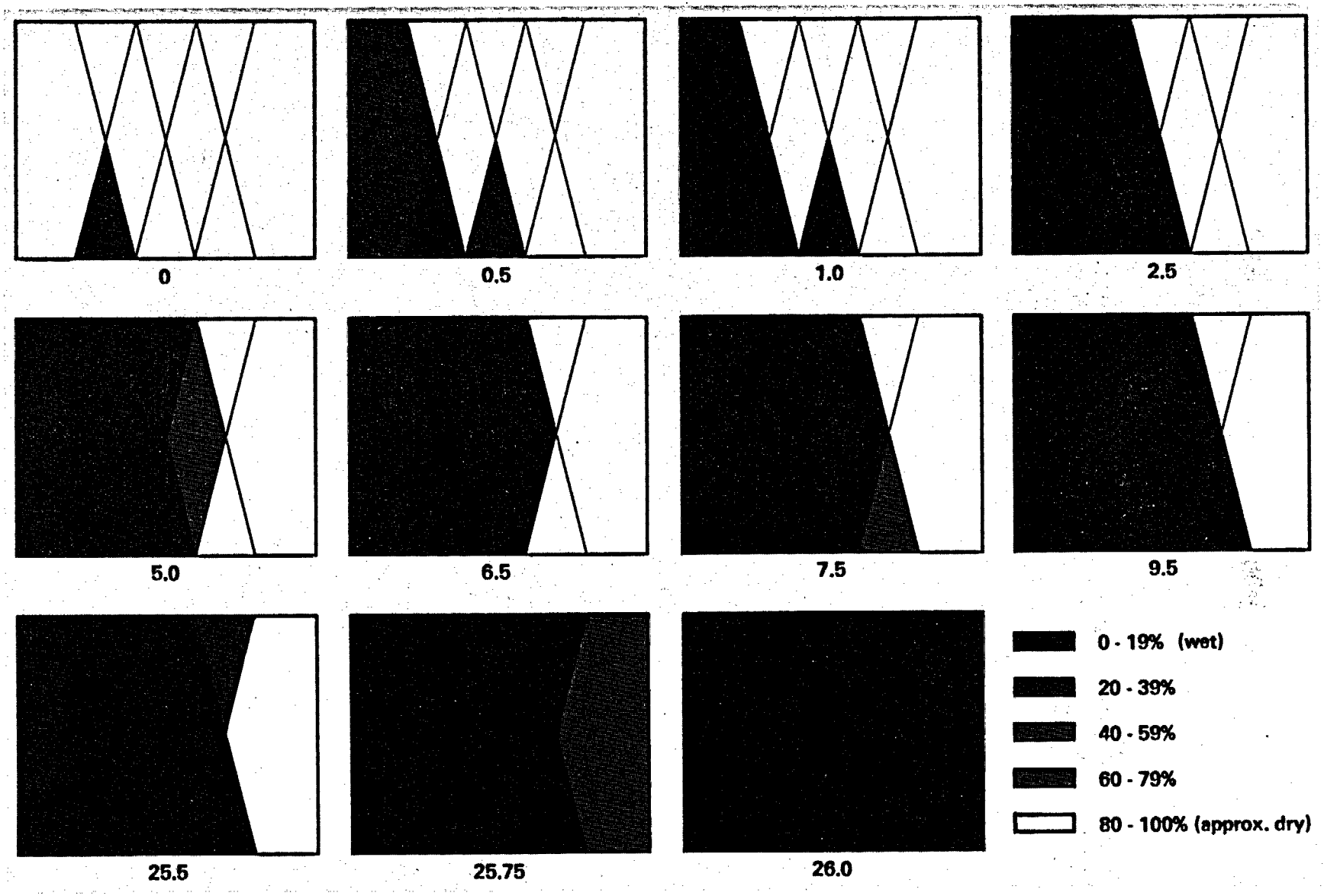
0
0.5
1.0
2.5
5.0
6.5
7.5
9.5
25.5
25.75
26.0
0 - 19% (wet)
20 - 39%
40 - 59%
60 - 79%
80 - 100% (approx. dry)

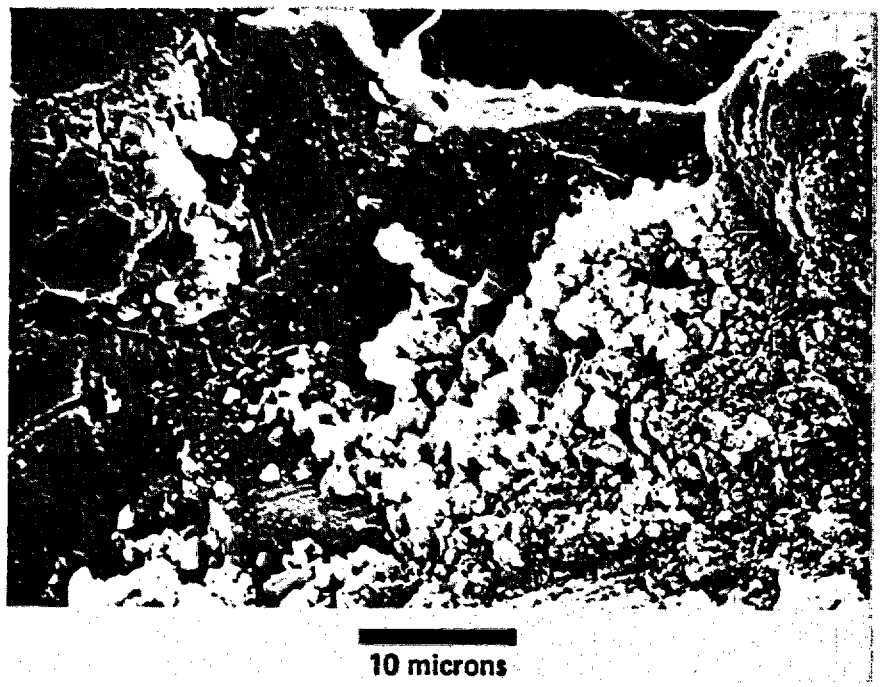
10 microns

Technical Information Department · Lawrence Livermore National Laboratory
University of California · Livermore, California 94550